Analysis of the Underwater Multi-Path Reflections on Doppler Shift Estimation

Zijun Gong, *Student Member, IEEE*, Cheng Li, *Senior Member, IEEE*, and Fan Jiang, *Member, IEEE*

***Abstract*—For underwater target localization and tracking, accurate Doppler shift estimation is very important. In this paper, the analysis of the multi-path effect on Doppler shift estimation accuracy is conducted for the narrow-band acoustic underwater channels. We conducted comprehensive analysis on the performance of a widely used low-complexity Doppler estimation algorithm, and showed that the mean square estimation error decreases with sample length quadratically. Then we derived the Cramér-Rao lower bound, which also decreases quadratically with sample length. As a result, we concluded that the impact of multi-path effect is negligible for a sampling length of several seconds. The theoretical results are verified by numerical simulations.**

***Index Terms*—Underwater, Doppler estimation, multi-path.**

I. Introduction

For many underwater applications, the localization and tracking of acoustic devices are based on Doppler shift measurements [1]–[5]. Generally, there are some location-aware devices distributed in the target area, referred to as anchors. The system can work in proactive or passive modes. In the proactive mode, anchors broadcast sinusoid waves at fixed frequencies. When a target moves into the surveillance area, it will reflect the sinusoid signals and the reflected signals will be received by the anchors. The movement of the target will add Doppler shifts to the reflected signals. By estimating the Doppler shifts, the anchors can keep tracking the target. In the passive mode, all the anchors are silent, while the target broadcasts a sinusoid wave at a fixed frequency. The anchors can then localize the target by receiving the signal and estimating the Doppler shift. This is a narrow band system, because the Doppler shifts varies in a very short range at the level of tens of Hz. In the conventional positioning systems, wide-band signals are generally employed to guarantee the ranging accuracy [6]. As comparison, the narrow-band system not only saves bandwidth for the other tasks, such as communications, but also allows multiple anchors to work simultaneously on different frequencies to provide diversity.

These anchors can be fixed or mobile. Compared with fixed anchors, mobile anchors have many advantages, such as good scalability, flexibility, and excellent coverage. As a matter of fact, autonomous underwater vehicles (AUVs) are very popular choices [7]–[12]. Suppose we have a target in the target area, and AUVs are moving on their predefined trajectories. The AUVs periodically broadcasts their real-time location information and sinusoid waves at fixed frequencies. The target can localize itself by decoding the beacon messages and estimating the Doppler shifts [5]. The localization accuracy is highly dependent on the Doppler estimation accuracy. For underwater channels, apart from the ambient noise, another important factor contributing to the Doppler estimation error is the multi-path effect. In this paper, we will derive the Cramér-Rao lower bound (CRLB) to show that the multi-path components' influence on estimation accuracy decreases quadratically as we increase the number of samples. However, this is only the theoretical lower bound. A more important question is how can we achieve it. A widely used low-complexity algorithm based on the DFT (Discrete Fourier Transform) will be introduced and comprehensive analysis will be conducted. The results show that the mean square estimation error of this algorithm also decreases quadratically as we increase the number of samples. We will also show that this algorithm approximately provides the maximum likelihood estimate (MLE) of Doppler shift through interpolation. For underwater acoustic signal processing, there are many mathematical tools more powerful than DFT, and they can deal with time-variant channels better. However, DFT achieves great balance between accuracy and efficiency in our case, because we are dealing with narrow-band signals, and the system parameters can be viewed as constant for the sampling time.

The remaining part of this paper is organized as follows. In Section II, the system model and the Doppler estimation algorithm are introduced. In Section III, comprehensive performance analysis is conducted, in terms of Doppler estimation error and the CRLB. The theoretical results will be verified by the simulations in Section IV, and Section V concludes the paper.

II. System Model and Doppler Estimation

A. System Model

For an arbitrary AUV moving at a fixed velocity and broadcasting a sinusoid wave at f_c Hz, the received signal at the target will be

$$r(t) = \sum_{b=1}^{B} A_b \sin\left(2\pi(f_c + f_{D,b})t + \theta_b\right) + w(t), \qquad (1)$$

where B is the number of paths between the AUV and the target. A_b, $f_{D,b}$ and θ_b are the amplitude, Doppler shift and a random phase delay of the b-th path. Without loss of generality, we assume $b = 1$ denotes the line-of-sight (LoS) path. In this

Z. Gong and C. Li are with the Faculty of Engineering and Applied Science, Memorial University of Newfoundland, St. John's, NL, A1B 3X5, Canada (E-mail: {zijun.gong, licheng}@mun.ca).

F. Jiang is with the Wireless Information and Network Sciences Laboratory (WINSLab), Massachusetts Institute of Technology (MIT), Cambridge, MA, 02139, USA (E-mail: fjiang@mit.edu).

model, we are assuming that the Doppler shifts of different paths are constant over the sampling period, which has a length of several seconds. This is a very commonly used channel model for underwater localization and communication [13], [14], and the fundamental assumption is that the radial velocity of the AUV with respect to the target is constant during several seconds. This approximation is very accurate when the distance between the target and the AUV is much larger than the product of the radial velocity and sampling period. This is especially true with the development of the CAS (Continuous Active Sonar) in recent years, which makes it possible to detect the targets tens and hundreds of kilometers away [15]. $w(t)$ denotes additive white Gaussian noise, which is a reasonable assumption for narrow-band underwater acoustic systems [16]. For localization applications, *a prior* information concerning the reflected signals is generally unavailable, and only the LoS path contains information about the target's location and velocity. Multi-path components are thus viewed as interference, and they will deteriorate the Doppler estimation accuracy.

From (33), it is clear that the received signal is the superposition of multiple sinusoid waves with different Doppler shifts, and our objective is to estimate the Doppler shift of the LoS path. After sampling the signal at f_s Hz in (33) ($f_s > 2(f_c + f_{D,1})$), the obtained sequence will be

$$\mathbf{r}[n] = \sum_{b=1}^{B} A_b \sin(\omega_b n + \theta_b) + \mathbf{w}[n], \tag{2}$$

where $\omega_b = 2\pi(f_c + f_{D,b})/f_s$. $\mathbf{w}$ is the noise vector, and the elements are zero-mean Gaussian variables with an identical variance of σ^2.

Given that f_s is larger than $2(f_c + f_{D,1})$, the estimation of $f_{D,1}$ is equivalent to the estimation of ω_1. A general approach is to conduct the discrete time Fourier transform (DTFT) on the received vector, and we can obtain $R(\omega) = \mathrm{DTFT}\{\mathbf{r}\}$. In $R(\omega)$, every path can be approximated by a sinc function, and our objective is to estimate the peak of the sinc function corresponding to the LoS signal. In the next section, we will briefly introduce a widely adopted low-complexity algorithm for this purpose.

B. Algorithm Description

As we can see in Appendix A, for a sinusoid wave, the MLE of the frequency can be obtained by identifying the peak of the received signal's Fourier transform. If we conduct DFT on the sampled sequence, only discrete spectrum can be obtained. We can of course increase the accuracy by over-sampling the spectrum (i.e., zero-padding before DFT). However, we will introduce a low-complexity algorithm in this part that can avoid all these troubles. The basic idea is to first find the largest two samples in the main lobe of the spectrum, and then estimate the peak's accurate position through interpolation.

To simplify the mathematical model and intuitively show how this algorithm works, we consider the scenario where only two major paths exist between the transmitter and receiver: the LoS path and one reflected path. The received signal will be

$$\mathbf{r}[n] = A_1 \sin(\omega_1 n + \theta_1) + A_2 \sin(\omega_2 n + \theta_2) + \mathbf{w}[n]. \tag{3}$$

Assume the sequence length is N, and the DFT of $\mathbf{r}$ is

$$\mathbf{r}_\omega[k] = \frac{1}{N} \sum_{n=0}^{N-1} \mathbf{r}[n] e^{-jkn\omega_0}, \tag{4}$$

where $\omega_0 = 2\pi/N$. There always exist $\beta_1, \beta_2 \in [0, 1)$ and $l_1, l_2 \in \{0, 1, \cdots, N-1\}$ that guarantee $\omega_1/\omega_0 = l_1 + \beta_1$ and $\omega_2/\omega_0 = l_2 + \beta_2$. The k-th element in $\mathbf{r}_\omega$ is given in (5), where $\theta_{i,k}$ and $\tilde{\theta}_{i,k}$ are phase shifts. $\mathbf{w}_\omega$ is the DFT of $\mathbf{w}$, and its elements are uncorrelated zero-mean Gaussian variables, with an identical variance of σ^2/N. For $k \in \{0, 1, \cdots, \lfloor N/2 \rfloor\}$, the second and forth components in (5) are negligible, and we have the following approximation

$$\begin{aligned} \mathbf{r}_\omega[k] \approx & \frac{A_1}{2N} e^{j\theta_{1,k}} \frac{\sin[(l_1 + \beta_1 - k)\pi]}{\sin[(l_1 + \beta_1 - k)\pi/N]} + \\ & \frac{A_2}{2N} e^{j\theta_{2,k}} \frac{\sin[(l_2 + \beta_2 - k)\pi]}{\sin[(l_2 + \beta_2 - k)\pi/N]} + \mathbf{w}_\omega[k]. \end{aligned} \tag{6}$$

The envelop of $\mathbf{r}_\omega$ is the superposition of two sinc functions, corresponding to the LoS and reflected paths. The main lobe of the LoS path can be identified by finding the peak value, because we can safely assume the LoS path is stronger than the reflected one. There are two samples in the main lobe of the LoS signal, and the indexes of them are l_1 and $l_1 + 1$.

If we further ignore the noise and multi-path components, (6) can be approximated by

$$|\mathbf{r}_\omega[l_1]| \approx \frac{A_1 \sin(\beta_1 \pi)}{2\beta_1 \pi}, \; |\mathbf{r}_\omega[l_1 + 1]| \approx \frac{A_1 \sin(\beta_1 \pi)}{2(1 - \beta_1)\pi}. \tag{7}$$

Based on $\mathbf{r}_\omega[l_1]$ and $\mathbf{r}_\omega[l_1 + 1]$, β_1 can be estimated as

$$\hat{\beta}_1 = \frac{|\mathbf{r}_\omega[l_1 + 1]|}{|\mathbf{r}_\omega[l_1 + 1]| + |\mathbf{r}_\omega[l_1]|}, \tag{8}$$

and ω_1 can then be computed as $\hat{\omega}_1 = (l_1 + \hat{\beta}_1)\omega_0$. The Doppler shift is obtained as $\hat{f}_{D,1} = \hat{\omega}_1 f_s/(2\pi) - f_c$. The estimation of l_1 must be done very carefully, and the interested readers are referred to [5] for more details. As we can see, a very important assumption of this algorithm is that the main lobe of the spectrum of a sinusoid wave can be well approximated by a sinc function, which allows us to conduct interpolation based on the two strongest samples.

III. Multi-path Effect Analysis

A. Error Analysis

Same to Section II-B, we will consider the scenario for $B = 2$ in (6), and employ $\mathbf{r}_\omega[l_1]$ and $\mathbf{r}_\omega[l_1 + 1]$ for the Doppler estimation. As we can see, these two samples in the main lobe of the LoS signal are contaminated by both noise and multi-path components. However, we can prove that as the number of samples increases, the noise component decreases linearly, while the strength of the interference from multi-path effect is inversely proportional to N^2. Taking the multi-path component in $\mathbf{r}_\omega[l_1]$ as an example (i.e., the third component in (31) for $k = l_1$), the strength is

$$\gamma = \left| \frac{A_2}{2N} e^{j\theta_{2,l_1}} \frac{\sin[(l_2 + \beta_2 - l_1)\pi]}{\sin[(l_2 + \beta_2 - l_1)\pi/N]} \right|^2. \tag{9}$$

$$\begin{aligned}\mathbf{r}_\omega[k] =& \frac{A_1 e^{j\theta_{1,k}}}{2N}\frac{\sin[(l_1+\beta_1-k)\pi]}{\sin[(l_1+\beta_1-k)\pi/N]} - \frac{A_1 e^{j\tilde{\theta}_{1,k}}}{2N}\frac{\sin[(-l_1-\beta_1-k)\pi]}{[\sin(-l_1-\beta_1-k)\pi/N]} + \\ & \frac{A_2 e^{j\theta_{2,k}}}{2N}\frac{\sin[(l_2+\beta_2-k)\pi]}{\sin[(l_2+\beta_2-k)\pi/N]} - \frac{A_2 e^{j\tilde{\theta}_{2,k}}}{2N}\frac{\sin[(-l_2-\beta_2-k)\pi]}{\sin[(-l_2-\beta_2-k)\pi/N]} + \mathbf{w}_\omega[k],\end{aligned} \tag{5}$$

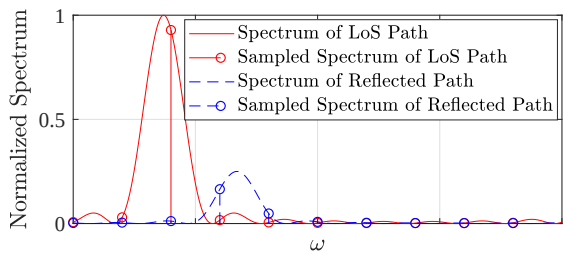

Fig. 1: The impact of the reflected path.

For $|x| < \pi/2$, we have $1 \geq |\sin(x)| \geq |2x/\pi|$. As a result, γ is bounded by

$$\gamma \leq \frac{A_2^2}{4N^2\left|2(l_2+\beta_2-l_1)/N\right|^2} = \frac{A_2^2}{16(l_2+\beta_2-l_1)^2}. \tag{10}$$

l_1, β_2 and l_2 are related to the sample number:

$$\begin{aligned} l_1 &= \omega_1/\omega_0 - \beta_1 = \frac{N\omega_1}{2\pi} - \beta_1, \\ l_2+\beta_2 &= \omega_2/\omega_0 = \frac{N\omega_2}{2\pi}. \end{aligned} \tag{11}$$

As a result, we have the upper bound of γ as

$$\gamma_{sup} = \frac{A_2^2\pi^2}{4N^2(\omega_2-\omega_1+\beta_1\omega_0)^2}. \tag{12}$$

When the sample number is very large, we have

$$\lim_{N\to\infty} N^2\gamma_{sup} = \frac{A_2^2\pi^2}{4(\omega_2-\omega_1)^2}. \tag{13}$$

Equivalently, we have the asymptotic limit of the interference as

$$\gamma_{sup} \to \frac{A_2^2\pi^2}{4N^2(\omega_2-\omega_1)^2}. \tag{14}$$

That is to say, as the number of samples increases, the interference strength is inversely proportional to N^2. Therefore, for very long sequences, noise dominates and multi-path interference is not a huge problem. To understand this, we should notice that we are only using the two samples in the main lobe of the LoS signal for Doppler estimation, which serves as a filter and filters out most multi-path components. This effect can be clearly observed in Figure 1. Inside the main lobe of the LoS signals, there are two samples from the side lobes of the multi-path component, which are very weak. The main lobe of the reflected path has been filtered out.

The analyses in this part are based on the assumption that the main lobes of different paths are well separated in frequency domain. If this is not the case, more complicated algorithms should be employed. For example, the Matching Pursuit algorithms can be used to iteratively isolate the paths, which will give us initial estimates of the parameters of different paths. Then, many numerical algorithms, such as Gradient Descent and Newton methods, can be used to obtain the maximum likelihood estimate.

B. CRLB Analysis

In this section, we will derive the CRLB of Doppler estimation error based on (2). In (2), there are totally $3B$ unknowns from B paths. We can put them in a vector as $\boldsymbol{\phi} = [\boldsymbol{\phi}_1^T, \boldsymbol{\phi}_2^T, \cdots, \boldsymbol{\phi}_B^T]^T$ for $\boldsymbol{\phi}_b = [\omega_b, A_b, \theta_b]^T$.

The conditional PDF of the received vector is

$$f(\mathbf{r}|\boldsymbol{\phi}) = (2\pi\sigma^2)^{-N/2}\exp\left(-\frac{|\mathbf{r}-\boldsymbol{\mu}|^2}{2\sigma^2}\right), \tag{15}$$

where $\boldsymbol{\mu} = E\{\mathbf{r}\}$ is given by $\boldsymbol{\mu}[n] = \sum_{b=1}^{B} A_b \sin(n\omega_b + \theta_b)$. The likelihood function is

$$l(\mathbf{r}|\boldsymbol{\phi}) = \ln(f(\mathbf{r}|\boldsymbol{\phi})) = -\frac{N}{2}\ln(2\pi\sigma^2) - \frac{|\mathbf{r}-\boldsymbol{\mu}|^2}{2\sigma^2}. \tag{16}$$

The partial derivative is given as

$$\frac{\partial l}{\partial \boldsymbol{\phi}} = \frac{1}{\sigma^2}(\boldsymbol{\mu}-\mathbf{r})^T\frac{\partial \boldsymbol{\mu}}{\partial \boldsymbol{\phi}}. \tag{17}$$

As a result, the Fisher information matrix (FIM) can be derived as

$$\mathbf{F}_{\boldsymbol{\phi}} = E\left\{\frac{\partial l}{\partial \boldsymbol{\phi}}\frac{\partial l^T}{\partial \boldsymbol{\phi}}\right\} = \frac{1}{\sigma^2}\frac{\partial \boldsymbol{\mu}^T}{\partial \boldsymbol{\phi}}\frac{\partial \boldsymbol{\mu}}{\partial \boldsymbol{\phi}}, \tag{18}$$

in which Jacobian matrix is

$$\frac{\partial \boldsymbol{\mu}}{\partial \boldsymbol{\phi}} = \left[\frac{\partial \boldsymbol{\mu}}{\partial \boldsymbol{\phi}_1}, \frac{\partial \boldsymbol{\mu}}{\partial \boldsymbol{\phi}_2}, \cdots, \frac{\partial \boldsymbol{\mu}}{\partial \boldsymbol{\phi}_B}\right]. \tag{19}$$

We can derive the partial derivatives as

$$\begin{aligned} \frac{\partial \boldsymbol{\mu}[n]}{\partial \omega_b} &= nA_b\cos(n\omega_b+\theta_b), \\ \frac{\partial \boldsymbol{\mu}[n]}{\partial A_b} &= \sin(n\omega_b+\theta_b), \\ \frac{\partial \boldsymbol{\mu}[n]}{\partial \theta_b} &= A_b\cos(n\omega_b+\theta_b). \end{aligned} \tag{20}$$

$\mathbf{F}_{\boldsymbol{\phi}}^{-1}$ gives the lower bound of the estimation error of all $3B$ parameters. However, we are only interested in those of the LoS path. To isolate the information we are interested in, define $\tilde{\boldsymbol{\phi}} = [\boldsymbol{\phi}_2, \cdots, \boldsymbol{\phi}_B]$, and rewrite (18) as

$$\mathbf{F}_{\boldsymbol{\phi}} = \frac{1}{\sigma^2}\begin{bmatrix} \frac{\partial \boldsymbol{\mu}^T}{\partial \boldsymbol{\phi}_1}\cdot\frac{\partial \boldsymbol{\mu}}{\partial \boldsymbol{\phi}_1} & \frac{\partial \boldsymbol{\mu}^T}{\partial \boldsymbol{\phi}_1}\cdot\frac{\partial \boldsymbol{\mu}}{\partial \tilde{\boldsymbol{\phi}}} \\ \frac{\partial \boldsymbol{\mu}^T}{\partial \tilde{\boldsymbol{\phi}}}\cdot\frac{\partial \boldsymbol{\mu}}{\partial \boldsymbol{\phi}_1} & \frac{\partial \boldsymbol{\mu}^T}{\partial \tilde{\boldsymbol{\phi}}}\cdot\frac{\partial \boldsymbol{\mu}}{\partial \tilde{\boldsymbol{\phi}}} \end{bmatrix}. \tag{21}$$

Then, we can define $\mathbf{C}_{\phi_1\phi_1} = \left[\mathbf{F}_{\boldsymbol{\phi}}^{-1}\right]_{1:3,1:3}$, which is the lower bound of the estimation error of $\boldsymbol{\phi}_1$. Based on the *Simple Block Matrix Inversion Theorem* [17], it can be given as

$$\begin{aligned}&\sigma^2\mathbf{C}_{\phi_1\phi_1}^{-1}\\ =&\frac{\partial\boldsymbol{\mu}^T}{\partial\boldsymbol{\phi}_1}\frac{\partial\boldsymbol{\mu}}{\partial\boldsymbol{\phi}_1}-\frac{\partial\boldsymbol{\mu}^T}{\partial\boldsymbol{\phi}_1}\frac{\partial\boldsymbol{\mu}}{\partial\tilde{\boldsymbol{\phi}}}\left(\frac{\partial\boldsymbol{\mu}^T}{\partial\tilde{\boldsymbol{\phi}}}\frac{\partial\boldsymbol{\mu}}{\partial\tilde{\boldsymbol{\phi}}}\right)^{-1}\frac{\partial\boldsymbol{\mu}^T}{\partial\tilde{\boldsymbol{\phi}}}\frac{\partial\boldsymbol{\mu}}{\partial\boldsymbol{\phi}_1}.\end{aligned}\tag{22}$$

Now we investigate how the multi-path effect deteriorates system performance. To begin with, we conduct singular value decomposition (SVD) for the partial derivatives:

$$\frac{\partial\boldsymbol{\mu}}{\partial\boldsymbol{\phi}_1}=\mathbf{U}\boldsymbol{\Sigma}\mathbf{V}\text{ and }\frac{\partial\boldsymbol{\mu}}{\partial\tilde{\boldsymbol{\phi}}}=\tilde{\mathbf{U}}\tilde{\boldsymbol{\Sigma}}\tilde{\mathbf{V}}.\tag{23}$$

(22) can then be rewritten as

$$\sigma^2\mathbf{C}_{\phi_1\phi_1}^{-1}=\mathbf{V}^T\boldsymbol{\Sigma}^T\boldsymbol{\Sigma}\mathbf{V}-\mathbf{V}^T\boldsymbol{\Sigma}^T\mathbf{U}^T\tilde{\mathbf{U}}\tilde{\mathbf{U}}^T\mathbf{U}\boldsymbol{\Sigma}\mathbf{V}.\tag{24}$$

Take the inverse on both sides of (24), and we will get

$$\mathbf{C}_{\phi_1\phi_1}=\sigma^2\mathbf{V}^T\boldsymbol{\Sigma}^{-1}\left(\mathbf{I}-\mathbf{U}^T\tilde{\mathbf{U}}\tilde{\mathbf{U}}^T\mathbf{U}\right)^{-1}\boldsymbol{\Sigma}^{-1}\mathbf{V}.\tag{25}$$

Defining $\mathbf{v}_1=[\boldsymbol{\Sigma}^{-1}\mathbf{V}]_{:,1}$ and $\mathbf{R}=\mathbf{U}^T\tilde{\mathbf{U}}$, the lower bound of estimation error of ω_1 is

$$\begin{aligned}CRLB_{\omega_1}=&\sigma^2\mathbf{v}_1^T\left(\mathbf{I}-\mathbf{R}\mathbf{R}^T\right)^{-1}\mathbf{v}_1\\ =&\sigma^2\mathbf{v}_1^T\left(\mathbf{I}+\mathbf{R}\left(\mathbf{I}-\mathbf{R}^T\mathbf{R}\right)^{-1}\mathbf{R}^T\right)\mathbf{v}_1\\ \le&\sigma^2|\mathbf{v}_1|^2(1+\mathrm{tr}\{\mathbf{R}\left(\mathbf{I}-\mathbf{R}^T\mathbf{R}\right)^{-1}\mathbf{R}^T\}).\end{aligned}\tag{26}$$

If we conduct the SVD of $\mathbf{R}$ as $\mathbf{R}=\mathbf{U}_\mathbf{R}\boldsymbol{\Sigma}_\mathbf{R}\mathbf{V}_\mathbf{R}$, the last component in (5) can be further simplified as

$$\begin{aligned}\mathrm{tr}\{\mathbf{R}\left(\mathbf{I}-\mathbf{R}^T\mathbf{R}\right)^{-1}\mathbf{R}^T\}=&\mathrm{tr}\left\{\left(\mathbf{I}-\boldsymbol{\Sigma}_\mathbf{R}^2\right)^{-1}\boldsymbol{\Sigma}_\mathbf{R}^2\right\}\\ \le&\mathrm{tr}\left\{\boldsymbol{\Sigma}_\mathbf{R}^2\right\}\\ =&\mathrm{tr}\left\{\mathbf{R}\mathbf{R}^T\right\}.\end{aligned}\tag{27}$$

As a result, we have the following inequality:

$$CRLB_{\omega_1}\le\sigma^2|\mathbf{v}_1|^2(1+\mathrm{tr}\{\mathbf{R}\mathbf{R}^T\}).\tag{28}$$

At the absence of the multi-path effect, if we denote the CRLB of ω_1 as $\overline{CRLB}_{\omega_1}$, we have $\overline{CRLB}_{\omega_1}=\sigma^2|\mathbf{v}_1|^2$. With multi-path comments, the lower bound increases by a factor of $1+\mathrm{tr}\{\mathbf{R}\mathbf{R}^T\}$, as we can see in (28). However, we want to point out that $\mathrm{tr}\{\mathbf{R}\mathbf{R}^T\}$ decreases very fast with the increase of the sample number, and is thus negligible. To see that, recall (23), in which $\mathbf{U}$ and $\tilde{\mathbf{U}}$ contain the eigenvectors of $\frac{\partial\boldsymbol{\mu}}{\partial\boldsymbol{\phi}_1}$ and $\frac{\partial\boldsymbol{\mu}}{\partial\tilde{\boldsymbol{\phi}}}$, respectively. Noticing that the column vectors in $\frac{\partial\boldsymbol{\mu}}{\partial\boldsymbol{\phi}_1}$ and $\frac{\partial\boldsymbol{\mu}}{\partial\tilde{\boldsymbol{\phi}}}$ are asymptotically orthogonal, which indicates the asymptotic orthogonality of the corresponding subspaces. That is to say, as the number of samples increases, the elements in $\mathbf{R}$ are very small, and the multi-path effect is negligible.

IV. Numerical Results

In the simulations, the target is located on the seabed, at the depth of 500 meters, while an AUV is moving in a random direction at 3 m/s.The AUV is 100 meters away from the seabed, and its horizonal distance to the target is two kilometers. f_c is chosen as 10 kHz, and $f_s=4f_c$. The sampling time T varies from 1 to 10 seconds at the step of one second. $B=3$ is considered, because there are generally two strong reflected paths from the bottom and surface of the sea. Denote the AUV's velocity as v, and we can define the maximum Doppler shift as $f_{D,\max}=f_cv/c$. The Doppler shifts of the two reflected paths are uniformly distributed between $-f_{D,\max}$ and $f_{D,\max}$. The average strength of the reflected signals is -10 dB (with respect to the LoS path), and follows the log-normal distribution with a standard deviation of 3 dB. The phase shifts of different paths are uniformly distributed between 0 and 2π. For the simulation parameters, the Doppler shifts of different paths are actually time variant. However, based on the numerical result, the Doppler shift of the LoS path only varies by around 10^{-3} Hz during the sampling time, which is negligible.

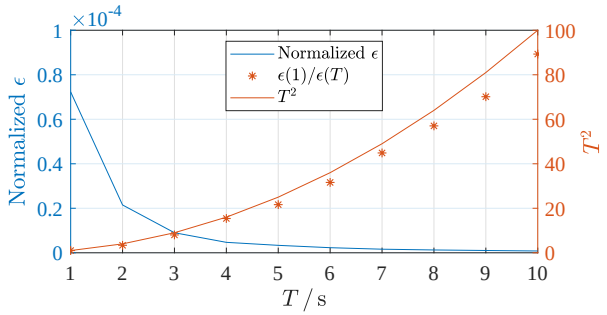

Fig. 2: Normalized ϵ for different sampling time.

In Figure 2, $\epsilon(T)$ is the average interference from the multi-path components for a sampling time of T seconds. In the figure, it is normalized by the signal strength of the LoS signal, and we can see the result decreases continuously with the increase of T. As we have mentioned, it should be inversely proportional to the N^2. Because $N=f_sT$, we should have $\epsilon\propto 1/T^2$. To see this, we plot $\epsilon(1)/\epsilon(T)$ versus T^2. Take $T=10$ as example, $\epsilon(1)/\epsilon(10)$ is equal to 100, which means the interference strength has decreased by 100 times when the sampling time increases by a factor of 10. $\epsilon(1)/\epsilon(T)$ and T^2 fit very well, which proves our conclusion.

In Figure 3, α is defined as $\alpha=CRLB_{\omega_1}/\overline{CRLB}_{\omega_1}-1$, and it indicates the increase of CRLB caused by multi-path effect. As we can see, α is inversely proportional to the sampling time, and thus the sample number. That is to say, this conclusion is generally true.

V. Conclusions

In this paper, we conducted comprehensive analysis of the multi-path effect on underwater Doppler estimation accuracy. The Doppler shift is assumed to be constant during several seconds. Based on the assumption of narrow-band acoustic channels, by deriving the CRLB, we showed that the multi-path interference decreases very fast with the increase of the sample number. It is also shown that a very simple algorithm can be used to achieve the performance bound. Both theoretical and numerical results show that the multi-path interference decreases quadratically with sample sequence length, for a sampling time of several seconds.

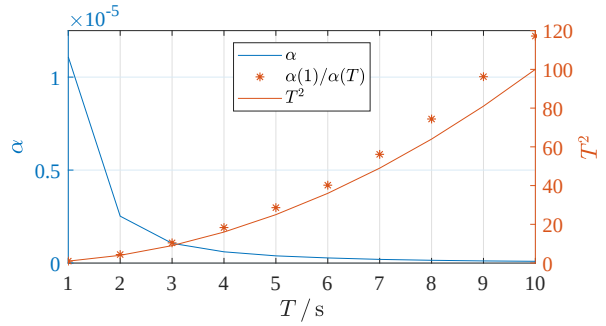

Fig. 3: The multi-path incurred CRLB increase for different sampling time.

APPENDIX A
MLE OF FREQUENCY

For a sinusoid wave, we will show that the MLE of its frequency is *almost* independent from its phase. Suppose we have a noisy sinusoid wave given by $r(t) = A\sin(\omega t + \theta) + w(t)$ for $t \in [0, T]$, where A is the amplitude, $\omega = 2\pi f$ is the frequency in radian, θ is the random phase, and $w(t)$ is additive Gaussian noise with a variance of σ^2. The MLE of the parameters A, f, and θ can be given by

$$[\hat{A}, \hat{\omega}, \hat{\theta}] = \arg\min_{\bar{A},\bar{\omega},\bar{\theta}} \int_{t=0}^{T} |r(t) - \bar{A}\sin(\bar{\omega}t + \bar{\theta})|^2 dt. \quad (29)$$

For any $\bar{\omega}$ and $\bar{\theta}$, $\bar{A}$ can be chosen to minimize the target function as

$$\hat{A} = \frac{\int_{t=0}^{T} r(t)\sin(\bar{\omega}t + \bar{\theta})}{\int_{t=0}^{T} \sin^2(\bar{\omega}t + \bar{\theta})}, \quad (30)$$

and the optimization problem is equivalent to

$$[\hat{\omega}, \hat{\theta}] = \arg\max_{\bar{\omega},\bar{\theta}} \frac{\left|\int_{t=0}^{T} r(n)\sin(\bar{\omega}t + \bar{\theta})dt\right|}{\int_{t=0}^{T} \sin^2(\bar{\omega}t + \bar{\theta})dt}. \quad (31)$$

In (31), we have

$$\int_{t=0}^{T} \sin^2(\bar{\omega}t + \bar{\theta})dt = \frac{T}{2} + \frac{1}{4\bar{\omega}}\left(\sin(2\bar{\omega}T + 2\bar{\theta}) - \sin(2\bar{\theta})\right).$$

For $Tf \ll 1$ or $T\omega \ll 2\pi$, we have

$$\int_{t=0}^{T} \sin^2(\bar{\omega}t + \bar{\theta})dt \approx \frac{T}{2}, \quad (32)$$

and this approximation is very accurate. That is to say, the MLE of $\bar{\omega}$ and $\bar{\theta}$ can be approximated by

$$\begin{aligned}[\hat{\omega}, \hat{\theta}] &\approx \arg\max_{\bar{\omega},\bar{\theta}} \left|\int_{t=0}^{T} r(t)\sin(\bar{\omega}t + \bar{\theta})dt\right| \\ &= \arg\max_{\bar{\omega},\bar{\theta}} \left|R(-\bar{\omega})e^{j\bar{\theta}} + R(\bar{\omega})e^{-j\bar{\theta}}\right|,\end{aligned} \quad (33)$$

where $R(\cdot)$ is the Fourier transform of $r(t)$. In our case, ω is positive, so we are trying to find $\bar{\omega} > 0$ that minimize the left hand side of (33). In this period, we have $|R(-\bar{\omega})| \ll 0$. As a result, we can again approximate the MLE as

$$[\hat{\omega}, \hat{\theta}] \approx \arg\max_{\bar{\omega},\bar{\theta}} \left|R(\bar{\omega})e^{-j\bar{\theta}}\right| = \arg\max_{\bar{\omega}} |R(\bar{\omega})|. \quad (34)$$

Apparently $\bar{\theta}$ is irrelevant and we have the maximum likelihood estimate of ω as

$$\hat{\omega} \approx \arg\max_{\bar{\omega},\bar{\theta}} \left|R(\bar{\omega})e^{-j\bar{\theta}}\right| = \arg\max_{\bar{\omega}} |R(\bar{\omega})|. \quad (35)$$

From here, we can see that the MLE of ω is independent from both A and θ. We can thus directly conduct Fourier transform on the received signal, and by finding the peak, we will very closely obtain the MLE of the frequency.

REFERENCES

[1] P. A. M. de Theije and J. . Sindt, "Single-ping target speed and course estimation using a bistatic sonar," *IEEE Journal of Oceanic Engineering*, vol. 31, no. 1, pp. 236–243, Jan. 2006.
[2] R. Diamant, L. M. Wolff, and L. Lampe, "Location tracking of ocean-current-related underwater drifting nodes using Doppler shift measurements," *IEEE Journal of Oceanic Engineering*, vol. 40, no. 4, pp. 887–902, Oct. 2015.
[3] P. Carroll, K. Domrese, H. Zhou, S. Zhou, and P. Willett, "Doppler-aided localization of mobile nodes in an underwater distributed antenna system," *Physical Communication*, vol. 18, pp. 49–59, 2016.
[4] R. Spindel, R. Porter, W. Marquet, and J. Durham, "A high-resolution pulse-Doppler underwater acoustic navigation system," *IEEE Journal of Oceanic Engineering*, vol. 1, no. 1, pp. 6–13, Sept. 1976.
[5] Z. Gong, C. Li, F. Jiang, and J. Zheng, "AUV-aided localization of underwater acoustic devices based on Doppler shift measurements," *IEEE Transactions on Wireless Communications*, vol. 19, no. 4, pp. 2226–2239, April 2020.
[6] Y. Shen and M. Z. Win, "Fundamental limits of wideband localization—part I: A general framework," *IEEE Transactions on Information Theory*, vol. 56, no. 10, pp. 4956–4980, Oct. 2010.
[7] M. Erol, L. F. M. Vieira, and M. Gerla, "AUV-aided localization for underwater sensor networks," in *International Conference on Wireless Algorithms, Systems and Applications (WASA 2007)*, Chicago, Illinois, USA, Aug. 2007, pp. 44–54.
[8] D. Mirza and C. Schurgers, "Collaborative localization for fleets of underwater drifters," in *OCEANS 2007*, Vancouver, BC, Canada, Sept. 2007, pp. 1–6.
[9] M. Waldmeyer, H. Tan, and W. K. G. Seah, "Multi-stage AUV-aided localization for underwater wireless sensor networks," in *2011 IEEE Workshops of International Conference on Advanced Information Networking and Applications*, March 2011, pp. 908–913.
[10] H. Maqsood, N. Javaid, A. Yahya, B. Ali, Z. A. Khan, and U. Qasim, "Mobil-AUV: AUV-aided localization scheme for underwater wireless sensor networks," in *2016 10th International Conference on Innovative Mobile and Internet Services in Ubiquitous Computing (IMIS)*, July 2016, pp. 170–175.
[11] R. Diamant and L. Lampe, "Underwater localization with time-synchronization and propagation speed uncertainties," *IEEE Transactions on Mobile Computing*, vol. 12, no. 7, pp. 1257–1269, July 2013.
[12] Z. Gong, C. Li, and F. Jiang, "AUV-aided joint localization and time synchronization for underwater acoustic sensor networks," *IEEE Signal Processing Letters*, vol. 25, no. 4, pp. 477–481, April 2018.
[13] Y. Zhao, H. Yu, G. Wei, F. Ji, and F. Chen, "Parameter estimation of wideband underwater acoustic multipath channels based on Fractional Fourier Transform," *IEEE Transactions on Signal Processing*, vol. 64, no. 20, pp. 5396–5408, Oct. 2016.
[14] B. Li, S. Zhou, M. Stojanovic, L. Freitag, and P. Willett, "Multicarrier communication over underwater acoustic channels with nonuniform Doppler shifts," *IEEE Journal of Oceanic Engineering*, vol. 33, no. 2, pp. 198–209, April 2008.
[15] R. van Vossen, S. P. Beerens, and E. van der Spek, "Anti-submarine warfare with continuously active sonar," *Sea Technology*, vol. 52, no. 11, pp. 33–35, 2011.
[16] M. Stojanovic and J. Preisig, "Underwater acoustic communication channels: Propagation models and statistical characterization," *IEEE Communications Magazine*, vol. 47, no. 1, pp. 84–89, Jan. 2009.
[17] S. E. Jo, S. W. Kim, and T. J. Park, "Equally constrained affine projection algorithm," in *Proceedings of the 38th Asilomar Conference on Signals, Systems and Computers*, vol. 1, Pacific Grove, California, USA, November 2004, pp. 955–959.